ADVANCED FUNCTIONAL MATERIALS
www.afm-journal.de

Photochemical Patterning and Characterization of Mechanical Properties on Soft Materials

Jun H. Park, Patrick J. Grimes, Henry E. Symons, Nicoletta Braidotti, Sebastien Rochat, Mark S. Workentin,* and Pierangelo Gobbo**

Although different chemistries for the spatio-temporal localization of molecules and gradients of chemical signals within soft materials are now available, the achievement of spatio-temporal patterns of mechanical properties in such materials and their characterization remain considerable challenges. This study presents the syntheses of two novel photo-sensitive and thermoresponsive hydrogel systems, a photo-stiffening and a photo-softening hydrogel. Their potential for fabricating soft materials with patterned mechanical properties is then demonstrated by fabricating an actuator whose higher-order bending properties can be switched on with light, and by encoding mechanical properties for digital information encryption and storage. Microindentation and a custom-made data analysis software are essential for the characterization of all the materials. From a general perspective, this work opens a route to the fabrication of soft materials with patterned mechanical properties, addressing an important emerging challenge in soft materials science with applications in soft robotics and information encryption and storage.

1. Introduction

Research efforts have been extensively devoted to developing techniques and chemistries for achieving spatio-temporal control of molecular patterns in soft materials.[1] This progress has led to significant advancements in recreating functional biological environments, innovating soft actuators, and expanding memory devices to soft materials.[2] While research has primarily concentrated on achieving higher and higher resolution on the precise spatio-temporal localization of biomolecules and gradients of chemical signals (optical, pH, concentration gradients, etc.), the development of spatio-temporal patterns of mechanical properties and their precise characterization still remain a considerable challenge.[3] The capability to produce and precisely characterize soft materials with detailed patterns of mechanical properties would open up a plethora of new possibilities in materials science. For example they could lead to the development of advanced biological scaffolds that can mimic the details of the mechanical microenvironments found in vivo to influence cell behavior (adhesion, migration, differentiation, gene expression, etc.), or favor tissue growth and regeneration.[4] They could also allow for the fabrication of next-generation, soft-robotic actuators capable of higher-order mechanical tasks,[5] and for the encryption and storage of digital information that is invisible to the naked eye, but detectable with highly sensitive tactile sensors.[6]

To date, only a few works have been reported in the literature that directly address the challenge of generating and characterizing patterns of mechanical properties on soft materials. These patterned materials are generally employed as substrates for cell

J. H. Park, P. J. Grimes, H. E. Symons, S. Rochat
School of Chemistry
University of Bristol
Bristol BS8 1TS, UK
E-mail: s.rochat@bristol.ac.uk
J. H. Park, M. S. Workentin
Department of Chemistry
University of Western Ontario
London, Ontario N6A 5B7, Canada
E-mail: mworkent@uwo.ca
N. Braidotti, P. Gobbo
Department of Chemical and Pharmaceutical Sciences
University of Trieste
Trieste 34127, Italy
E-mail: pierangelo.gobbo@units.it
S. Rochat
School of Engineering Mathematics and Technology
University of Bristol
Bristol BS8 1TR, UK
P. Gobbo
National Interuniversity Consortium of Materials Science and Technology
Unit of Trieste
Via G. Giusti 9, Firenze 50121, Italy
The ORCID identification number(s) for the author(s) of this article can be found under https://doi.org/10.1002/adfm.202416095

DOI: 10.1002/adfm.202416095

biology.[7] The direct and detailed characterization of the intensive mechanical properties of the patterns (e.g., storage and loss moduli, rather than stiffness or relative stiffness changes), however, remains technologically difficult. Thus far, fluorescence microscopy methodologies have been used to indirectly visualize the patterns of mechanical properties on hydrogels by photocrosslinking their polymer networks and copolymerizing fluorescent molecules,[7a] or, vice versa, by photo-cleaving the polymer network and releasing fluorescent molecules.[7b] Although this method provides a visual inspection of the pattern, it lacks direct measurements of its mechanical properties. Another possible approach is to characterize the mechanical properties of a non-patterned, bulk material that has been exposed to the same irradiation conditions used for generating the pattern, but in the absence of the mask.[7b,c] At the base of this method, there is the assumption that the conditions used to generate the pattern produce the same changes in mechanical properties as the method used to fabricate the bulk sample. This is not always true due to different light attenuation dynamics that are intrinsic to the two different techniques. Moreover, with this method it is impossible to visualize a pattern.

An interesting method that is emerging for characterizing the mechanical properties of soft living or non-living matter is Brillouin microscopy. This technique is a non-contact imaging technique that acquires information on the mechanical properties of a sample by analyzing the scattering of light. It provides insights into material elasticity and viscosity at GHz frequencies, enabling the visualization of viscoelastic properties in three dimensions with high resolution.[8] While this technique holds promises for the direct characterization of patterns of mechanical properties, it still presents important limitations. In order to provide useful information, it requires precise knowledge of the local refractive index of the sample, which is not always possible especially when developing novel materials. It requires high-power pumping lasers and complex illumination and collection geometries that can make it difficult to measure certain samples. Finally, and most importantly, the physical-mechanical interpretation of Brillouin microscopy data is still heavily debated within the scientific community.[8a] Thus far the best method reported to characterize patterns of mechanical properties involves the use of atomic force microscopy (AFM). AFM can provide punctual measurements of the mechanical properties of a sample and therefore, by carrying out array-type measurements, it may allow for the mapping of patterns of mechanical properties.[7d,e,9] However, AFM measurements are highly influenced by localized surface features not associated with the mechanical pattern and can only provide detailed maps of small surface areas (microns squared).[10] Thus far, AFM has been used to determine relative stiffness changes across a patterned sample.

In this work, we report a novel strategy for the photochemical fabrication of patterns of mechanical properties in soft materials and for their precise characterization using microindentation. For this, we have developed two new types of photoresponsive and thermoresponsive poly-*N*-isopropylacrylamide (PNIPAM)-based hydrogels that enable the patterning of mechanical properties for diverse applications. The first hydrogel is a photo-stiffening system capable of spatio-temporally crosslinking by exploiting a light-induced, strain-promoted alkyne-azide cycloaddition (*hv*SPAAC) (**Figure 1a**). This rapid and highly selective photo-click reaction involves the photo-unmasking of cyclopropenone-masked dibenzocyclooctyne (*hv*DIBO) moieties with 365 nm light to produce strained alkynes that can efficiently cyclize in situ with available neighboring azide groups, forming triazoles.[11] In this photo-stiffening hydrogel system, the *hv*SPAAC reaction provides fast and excellent spatio-temporal control over cross-linking density, and grants the ability to increase the material's storage modulus. While *hv*DIBO has been utilized in a hydrogel system previously to pattern fluorophores, our study marks the first instance of its application to pattern mechanical properties in hydrogels.[12]

The second hydrogel is instead a photo-softening system capable of spatio-temporally decrosslinking with 365 nm light by exploiting an *ortho*-nitrobenzyl ester (*o*-NB) photo-cleaving mechanism (Figure 1b). The *o*-NB group has been widely used in biological applications – for example as a photo-labile protecting group for DNA architectures[13] and in the spatial control of protein binding on lipid membranes,[14] – as well as in materials chemistry – for example, in the development of drug delivery systems capable of photo-selective release of therapeutic agents.[15] In this work, the *o*-NB group was used to develop a photo-cleavable, PEG (polyethylene glycol)-based dimethacrylate crosslinker for hydrogels, which upon exposure to 365 nm light, caused the decrosslinking and softening of the polymer network. The viscoelastic behaviors of the photo-stiffening and photo-softening hydrogels were characterized by microindentation coupled to a custom software, called *ALIAS-Viscoelasticity*, for the automated analysis of thousands of indentation curves and the construction of maps of patterned mechanical properties.

In this work, for the indentation measurements, we utilized a micro-indenter equipped with a micro-electro-mechanical sensor (MEMS) with ± 2000 μN of force range and a noise floor of 0.005 μN. While there are a few attempts reported that use indentation to map patterns of mechanical properties on hydrogels in the literature,[16] the maps achieved so far present very low resolutions that make the generated patterns barely visible, making the interpretation of the experimental results difficult and hindering the development of technological applications. In contrast, our approach based on microindentation and *ALIAS-Viscoelasticity*, enabled us to perform high-resolution indentation mapping to visualize the details of photo-generated patterns, and to showcase potential applications of our method for the development of advanced soft actuators and for the encryption and storage of information in soft materials. Moreover, our methodology allowed us to obtain valuable insights into the physical-organic chemistry transformations occurring within the photo-reactive soft materials. From a general perspective, our approach sets a new paradigm in the extraction of mechanical information that can be spatio-temporally encoded into soft materials.

We then combined the two hydrogel systems into a single bilayered soft actuator, whose higher-order bending properties could be switched on with UV light. In this system, a homogenous light irradiation of the entire material caused an asymmetric change in the mechanical and diffusivity properties of the two layers. This change caused the bilayered actuator to pass from a simple thermally-induced, symmetrical contraction, to a complex bending motion, where by increasing the temperature, the material initially bent toward the photo-stiffening hydrogel layer, and

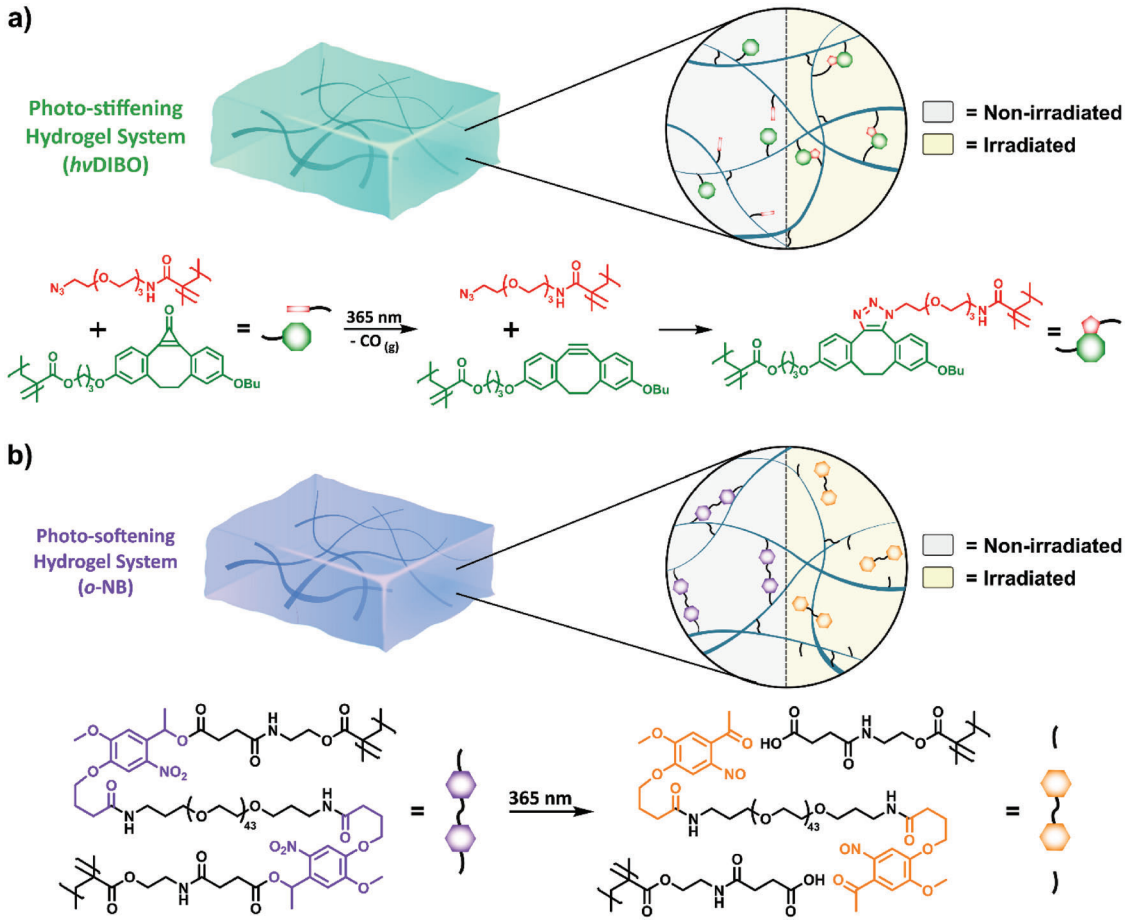

Figure 1. a) Scheme describing our photo-stiffening hydrogel system capable of spatio-temporally crosslinking via light-induced strain-promoted alkyne-azide cycloadditions (*hv*SPAAC). The blue lines inside the hydrogel representation depict the main PNIPAM polymer network and the small black lines in the magnified scheme are the *N*,*N*′-methylenebisacrylamide (MBAM) crosslinks. The *hv*DIBO groups (green octagons) can be photo-unmasked with 365 nm light to yield, in situ, the strained alkyne DIBO, which then crosslinks with the azide groups (red rectangles). b) Scheme describing our photo-softening hydrogel system capable of spatially and temporally softening via *ortho*-nitrobenzyl (*o*-NB) photo-cleavage reactions. The blue lines inside the hydrogel representation depict the main PNIPAM polymer network and the small black lines in the magnified scheme are the MBAM crosslinks. The *o*-NB moieties (purple hexagons) can undergo intramolecular rearrangements with 365 nm light to form cleaved aryl ketones (orange hexagons).

then began to straighten at higher temperatures. In the study of this system, microindentation was key in characterizing the viscoelastic and solvent diffusivity properties of the actuator, providing a comprehensive understanding of the material's response dynamics.

Finally, we showed that our photo-stiffening and photo-softening hydrogels could be utilized to store invisible digital information in the form of patterned mechanical properties. In information storage, numerous works have illustrated the encoding and decoding of information in stimuli-chromic, photoluminescent, solvent-responsive, and heterogeneous soft materials.[17] However, to the best of our knowledge, the encoding of mechanical properties on materials for information storage and encryption/decryption remains essentially unexplored. Patterns of mechanical properties are often invisible to the naked eye, enabling a powerful and secure way of storing information within soft materials. The encoded mechanical information could then be retrieved through careful microindentation mapping coupled with the automated analysis of a very large number of individual indentation curves (>5700) provided by our *ALIAS-Viscoelasticity* software.

2. Results and Discussion

2.1. Photo-Stiffening Hydrogel System

The *hv*DIBO monomer (2) (**Figure 3**) was made from a nucleophilic acyl substitution between methacryloyl chloride and *hv*DIBO (1), which was synthesized following a procedure reported by Luo et al. (Sections S1.2.1-2. and Scheme S1, Supporting Information).[18] The azide monomer (3) (**Figure 2a**) was similarly produced from commercially available methacryloyl chloride and 11-azido-3,6,9,12-tetraoxatetradecan-1-amine (Section S1.2.3., Supporting Information). Compounds (2) and (3) were fully characterized with ^{1}H and $^{13}C\{^{1}H\}$ nuclear magnetic resonance (NMR) spectroscopy, infrared (IR) spectroscopy, UV–vis spectroscopy, and electrospray ionization mass spectrometry (Figures S5–S12, Supporting Information).

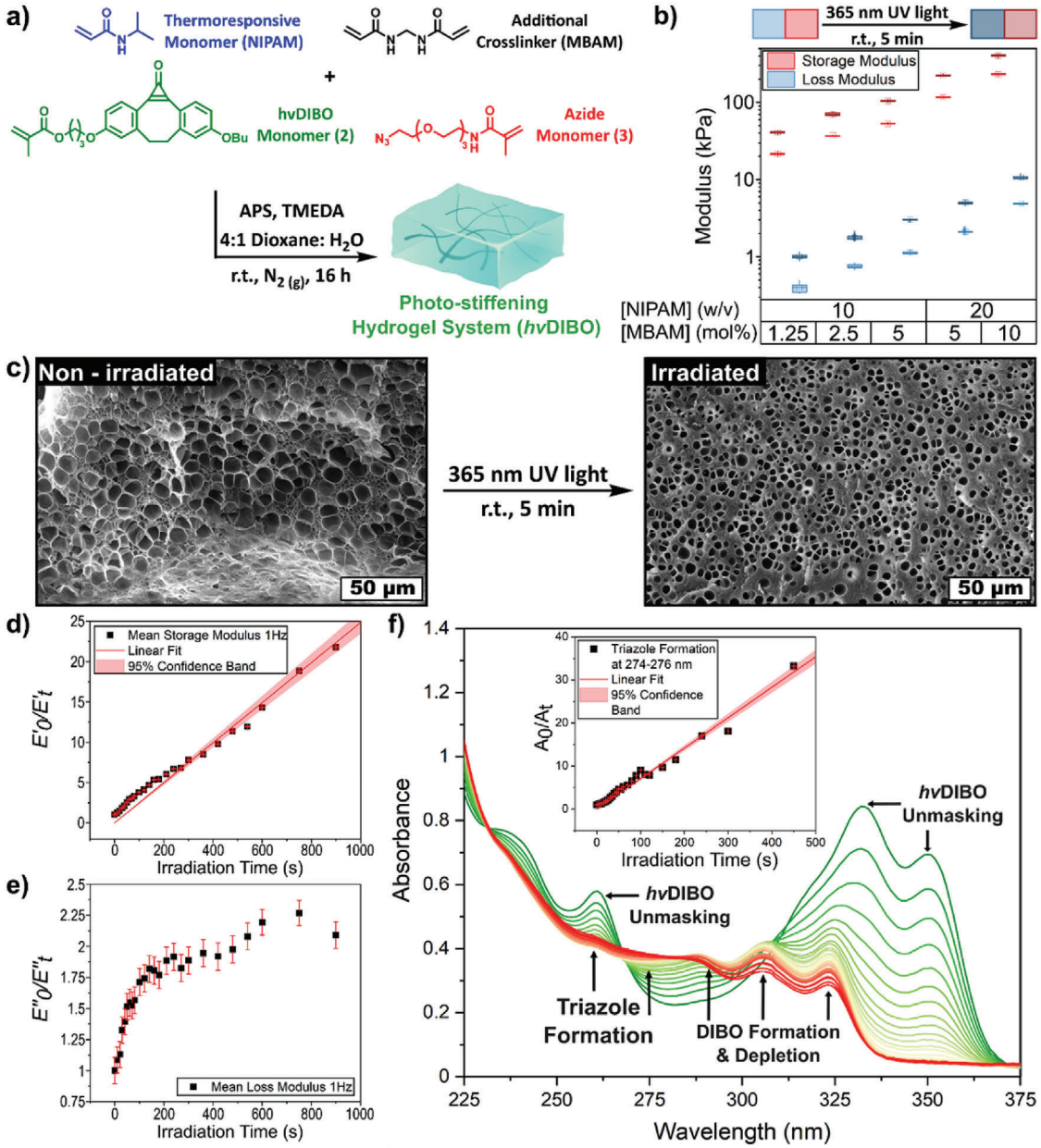

Figure 2. a) Synthesis of a photo-stiffening hydrogel (*hv*SPAAC) via the free radical hydrogelation of NIPAM, MBAM, *hv*DIBO methacrylate (2), and azide methacrylate (3) with APS and TMEDA. b) Storage (red) and loss (blue) moduli (kPa) box plot of five photo-stiffening hydrogels of different compositions (varying NIPAM and MBAM concentrations) obtained from microindentation analysis. The lighter colored boxes represent pre-irradiation moduli, and the darker colored boxes show the moduli after 5 min of 365 nm UV irradiation. c) SEM images of a critical point dried, photo-stiffening hydrogel ($5 \times 5 \times 1$ mm^3) that was sputter-coated with silver. Half of the hydrogel was not irradiated (left), and the other half was irradiated (right) with a 365 nm LED for 5 min with irradiance of ≈130 µW mm^{-2} (500x magnification, scale bar = 50 µm). d) Microindentation kinetics study plot of the irradiation (365 nm UV light in varied time increments for a total of 20 min) of a photo-stiffening hydrogel of dimensions $5 \times 5 \times 1$ mm^3. The reciprocal of the changes in the storage modulus (E') of the photo-stiffening hydrogel plotted against irradiation time and fit to a linear fit with a R-squared value of 0.982, indicating 2nd order reaction kinetics. The error bars represent the standard deviation of 4 measurements and the red band is a 95% confidence band of the fitting. e) The reciprocal of the change in loss modulus (E'') plotted against irradiation time with the error bars representing the standard deviation of 4 measurements. f) UV–vis kinetics study plots of the absorbance changes as a result of irradiation (365 nm UV light in varied time increments for a total of 20 min) for a thin, photo-stiffening hydrogel immobilized on a fused silica plate. The absorbance changes between 225–375 nm plotted as a function of irradiation time (s) for the *hv*DIBO photo-unmasking step (green to red traces indicate the experiment progression). *Inset*: The inverse of the change in the average absorbances for the SPAAC crosslinking reaction (black squares) was then plotted against irradiation time (s) to give a linear relationship with a R-squared value of 0.988, verifying the kinetics reaction order for this step to be 2nd order. The red error bars represent the standard deviation between the 3 wavelength absorbance changes at each time point and the red band is a 95% confidence band of the fitting.

The main component of the hydrogel was *N*-isopropylacrylamide (NIPAM) to confer thermoresponsive properties to the material (vide infra). In general, the photo-stiffening hydrogel was made via free radical hydrogelation using ammonium persulfate (APS) and tetramethylethylenediamine (TMEDA) as the radical initiator system due to their water solubility and function at ambient temperatures (Figure 2a and Figure S3, Supporting Information). Five hydrogel samples of dimensions 5 × 5× 1 mm^3 were prepared using this general procedure and by systematically varying the concentrations of NIPAM (10 or 20 w/v%) and MBAM [1.25, 2.5, 5 or 10 mol% with reference to (wrt.) NIPAM], while the concentrations of monomers (2) and (3) were held at 2 mol% wrt. NIPAM.

The viscoelastic properties of these samples were assessed using a microindenter. This evaluation aimed to discern how the initial mechanical properties of the hydrogel were influenced by the extent of photo-stiffening achieved through *hν*SPAAC crosslinking reactions (Section S1.2.5., Supporting Information). Increasing the concentration of NIPAM led to a significant rise in both the storage (E') and loss (E'') moduli of the hydrogel, which increased from to 53.7 ± 1.1 kPa (E') and 1.15 ± 0.06 kPa (E'') for the 10 w/v% NIPAM sample to 117.3 ± 3.2 kPa (E') and 2.15 ± 0.09 kPa (E'') for the 20 w/v% NIPAM sample (Figure 2b). In contrast, marginal increases in loss and storage moduli were noted by increasing the concentration of the MBAM crosslinker (Figure 2b). Interestingly, despite their different compositions, when the five hydrogel samples were irradiated with UV-A light (365 nm, irradiance of ≈130 μW mm^{-2}) for 5 min, all showed a comparable increase in their storage and loss moduli of 88 ± 9% and 140 ± 21%, respectively. This was attributed to the formation of triazole crosslinks (Figure 2a) within the pores of the pre-existing hydrogel matrix, which led to a comparable increase in crosslinking density across all hydrogel compositions. For the next experiments in this work, the composition of the photo-stiffening hydrogel was fixed to 10 w/v% NIPAM, 5 mol% MBAM, 2 mol% *hν*DIBO monomer (2), and 2 mol% azide monomer (3) because of the superior quality of this hydrogel. To further prove the efficiency of the *hν*SPAAC reaction, we prepared a new NIPAM-based hydrogel, masked half of it, and irradiated the other half with a UV LED (365 nm, irradiance of ≈130 μW mm^{-2}) for 5 min (Section S1.2.6., Supporting Information). After this experiment, the irradiated half of the hydrogel became slightly yellow and contracted. The hydrogel was then characterized via indentation and its viscoelastic properties were mapped across the sample (Figure S14, Supporting Information). The storage and loss modulus maps showed a defined divide between the irradiated and non-irradiated halves of the material.

The non-irradiated portion of the hydrogel had average storage and loss moduli of 50.2 ± 5.3 kPa and 2.14 ± 0.29 kPa, respectively, whereas the irradiated portion had average storage and loss moduli of 85.2 ± 4.5 kPa and 4.78 ± 0.39 kPa, respectively. The sample showed a drastic difference in viscoelasticity between the non-irradiated and irradiated portions, with the irradiated side having a 70 ± 16% greater average storage modulus and a 123 ± 28% greater average loss modulus than the non-irradiated side. This was attributed to the *hν*SPAAC reaction being triggered exclusively in the irradiated portion of the material, leading to additional triazole crosslinks that stiffened the hydrogel.

A hydrogel produced in the same way was then analyzed via scanning electron microscopy (SEM) imaging (Section S1.1.10., Supporting Information). Figure 2c and Figure S15 and S16 (Supporting Information) show a clear difference in porosity between the non-irradiated and irradiated halves of the material. The non-irradiated portion of the hydrogel exhibited an average pore area of 37.0 ± 18.2 μm^2 with tightly connected pores, whereas the irradiated half of the material had an average pore area of 9.9 ± 5.9 μm^2 with pores that were separated by compact polymeric material. Although the sample drying process may have slightly altered the microstructure of the material, it is evident that the UV irradiation has shrunk the hydrogel's pores by ≈73 ± 63% and condensed its matrix. These findings correlate well with the microindentation viscoelasticity maps and highlight the efficiency of the *hν*SPAAC reaction in stiffening the PNIPAM-based hydrogel.

Seeing these promising results, we next explored the use of microindentation analysis to characterize the hydrogel photocrosslinking reaction kinetics and gain insights on the chemical processes that were taking place inside the soft material. The results were then compared with an analogous kinetics study performed using UV–vis spectroscopy. Both kinetics studies were carried out by analyzing photo-stiffening hydrogels that were progressively irradiated with 365 nm UV light (≈130 μW mm^{-2}) over gradually increasing time intervals, starting from 10 s for a total of 20 min (Section S1.2.8., Supporting Information).

Indentation analysis (Figure S17a and b, Supporting Information) showed that the initial average storage and loss moduli of the hydrogel were 51.2 ± 1.8 kPa and 4.41 ± 0.32 kPa, respectively. Upon UV irradiation, the storage and loss moduli progressively increased to 140.4 ± 8.0 kPa and 6.84 ± 0.62 kPa, respectively, with ≈90% of the change completed after just 4 min of irradiation. The inverse of the change in storage modulus (E'_0/E'_t) over irradiation time was then plotted showing a linear trend (Figure 2d and Figure S17a, Supporting Information), which indicates that the mechanical stiffening of the hydrogel via the *hν*SPAAC was following 2nd order reaction kinetics. This agrees well with data reported in the literature that demonstrate that the *hν*SPAAC reaction has two steps: the first step is the photo-unmasking of the cyclopropenone group of *hν*DIBO to yield DIBO and carbon monoxide gas, and the second step is the formation of the triazole ring through the SPAAC reaction between the azide and photo-unmasked strained alkyne. The 2nd order reaction kinetics suggests the second step in the *hν*SPAAC reaction is the rate determining step, and this is expected as the first step is a unimolecular reaction, while the second step is a bimolecular reaction.[19]

In contrast, the inverse of the change in loss modulus (E''_0/E''_t) over irradiation time showed a linear trend only in the first 200 s (Figure 2e and Figure S17b, Supporting Information), after which the plot reached a plateau. This was possibly due to the hydrogel polymer network, that upon crosslinking, started to expel water progressively more slowly. This was supported by a reduction in the effective diffusivity of water through the material from 1.98 ± 0.04 × 10^{-9} to 1.19 ± 0.09 × 10^{-10} m^2 s^{-1}, also consistent with a reduction of average pore size as shown in Figure 2c. A control kinetics experiment was also performed with a hydrogel synthesized following the same procedure as the photo-stiffening hydrogel, but without using the *hν*DIBO

monomer (2). The same microindentation kinetics study was performed on this hydrogel showing no variation in the storage and loss moduli of the hydrogel upon irradiation with 365 nm UV light (Figure S17c, Supporting Information). This showed that the *hv*DIBO monomer (2) is critical for the photo-stiffening of the hydrogel.

The microindentation kinetics results were then compared to UV–vis kinetics data collected from a thin hydrogel (Figure S2, Supporting Information) that was formed on a silane-treated, fused silica slide (Section S1.1.5. and Figure S1, Supporting Information). The UV–vis absorbance spectrum of the sample was collected before irradiation, and it showed absorbance maxima at 261, 332, and 350 nm, which correspond to the *hv*DIBO moiety (Figure 2f).[20] Initially, upon UV irradiation of the sample (365 nm, ≈130 μW mm^{-2}), these absorbances began to decrease and new absorbance bands appeared at 288, 306, and 323 nm, representing the conversion of *hv*DIBO to DIBO (strained alkyne) groups via the photo-unmasking of the cyclopropenones. The DIBO absorbance bands then decreased as the strained alkynes began reacting with the available azides in the hydrogel's polymer matrix to form triazole crosslinks that absorb below 282 nm. The depletion of *hv*DIBO upon UV irradiation was monitored through the absorbance between 349–351 nm and plotted against irradiation time (Figure S18a, Supporting Information). The plot of the natural logarithm of the change in absorbance between 349–351 nm with irradiation time showed a linear trend, indicating, as expected, 1st order reaction kinetics.[21] The triazole formation was instead tracked by monitoring the absorbance changes between 274–276 nm with the irradiation time. The inverse of the change in absorbance between 274–276 nm ($A_{274\text{-}276\ nm,0}/A_{274\text{-}276\ nm,t}$) over irradiation time showed a linear trend, confirming 2nd order reaction kinetics for the SPAAC reaction.[20] The photo-crosslinking reaction monitored via UV–vis spectroscopy was found to be ≈90% complete after only 45 s of UV irradiation.

When comparing the microindentation kinetics experiment (≈90% completion in 4 min) with the UV–vis spectroscopy kinetics experiment (≈90% completion in 45 s), we observed that the microindentation kinetics was ≈5 times slower compared to the UV–vis kinetics. Since both kinetic studies were performed using the same irradiance, one rationale for the discrepancy in the reaction completion time is that the microindentation study measures the change in the mechanical properties of the material over irradiation time as a result of the light-induced SPAAC reaction, whereas UV–vis spectroscopy directly measures molecular reactivity within the transparent material. As such, it seems that there is a time delay between the chemical process and the contraction of the polymer network, most likely due to the rearrangement of the polymer chains. The UV–vis study was also carried out with a thin hydrogel sample (Figure S2, Supporting Information) to obtain spectra with absorbances below 1.5, while the microindentation kinetic study was conducted on a 1 mm thick sample to avoid the hard substrate contribution to the measured mechanical properties. From a general perspective, our data still demonstrates the possibility of using microindentation to elucidate the reaction kinetics mechanisms of chemical processes hosted within soft materials.

2.2. Photo-Softening Hydrogel System

At the heart of the photo-softening hydrogel system, there was the photo-cleaving, linear, dimethacrylate *o*-NB crosslinker (5) (Figure 3a). The dimethacrylate *o*-NB crosslinker (5) was synthesized by reacting a photo-cleavable, PEG-based crosslinker (4) (3 kDa) with 2-aminoethyl methacrylate (Section S1.3.1., Supporting Information).[22] The dimethacrylate *o*-NB crosslinker (5) was characterized using matrix-assisted laser desorption ionization – time of flight (MALDI-TOF) mass spectrometry, IR spectroscopy, UV–vis spectroscopy, and ^{1}H and ^{13}C {^{1}H} NMR spectroscopy (Figures S19–S23, Supporting Information).[22]

To synthesize photo-softening hydrogels, we used the same general procedure that was used for the photo-stiffening hydrogel (Figure 3a; Section S1.3.4., Supporting Information). In order to obtain pre- and post-irradiation storage and loss moduli values for the photo-softening hydrogel that were comparable to those of the photo-stiffening hydrogel, we carried out a small compositional study where we kept a 2:1 mol% ratio between *o*-NB crosslinker (5) and MBAM, and systematically increased the amount of crosslinker (5) and MBAM or increased the concentration of NIPAM. The viscoelastic properties of the hydrogel were then characterized using microindentation. Figure 3b shows that the storage and loss moduli of the photo-softening hydrogels could be varied from 1.50 ± 0.13 kPa (E') and 0.04 ± 0.01 kPa (E'') to 45.7 ± 4.2 kPa (E') and 1.89 ± 0.69 kPa (E''). In particular, the photo-softening hydrogel synthesized with 10 w/v% NIPAM, 3 mol% MBAM and 6 mol% of *o*-NB crosslinker (5) was selected as the most appropriate, as it had storage and loss moduli that were comparable to those of the photo-stiffening hydrogel described in the previous section (i.e., with composition 10 w/v% NIPAM, 5 mol % MBAM, 2 mol% *hv*DIBO monomer (2), and 2 mol% azide monomer (3)). Having comparable viscoelastic properties for the two types of hydrogels was important for the fabrication of a bilayered actuator (vide infra).

As a result of the two photo-cleavable *o*-NB moieties within the *o*-NB crosslinker (5), the level of cross-linking could be precisely reduced with a high degree of spatio-temporal control using 365 nm light. Although *o*-NB has been used in photo-softening hydrogels previously, a PNIPAM-based hydrogel has not been crosslinked with an *o*-NB crosslinker before.[23] *o*-NB groups generally exhibit a broad absorption, with λ_{max} = 350 nm, but are susceptible to reaction across a wide range of wavelengths, extending from below 350 nm to beyond 400 nm.[23] On irradiation with UV light, the reactive *aci*-nitro functionality is formed from the nitro group when a proton is abstracted from the adjacent benzylic carbon. An irreversible formation of a 5-membered ring follows, the subsequent cleavage of which yields a carboxylic acid and *o*-nitrosobenzaldehyde as products. This frees the carboxylic acid group from the rest of the PEG chain and enables photo-cleavage of the crosslinker (Scheme S5, Supporting Information).[24] Upon UV irradiation (365 nm for 30 min, ≈130 μW mm^{-2}), the optimized photo-softening hydrogel (i.e., with composition 10 w/v% NIPAM, 3 mol% MBAM and 6 mol% of *o*-NB crosslinker (5)) became dark yellow in color, and its storage modulus decreased from 45.7 ± 4.2 kPa to 2.22 ± 0.35 kPa, while its loss modulus decreased from 1.89 ± 0.69 kPa to 0.21 ± 0.08 kPa. Notably, this corresponds to decreases of 95 ± 13% and 89 ± 49%, respectively.

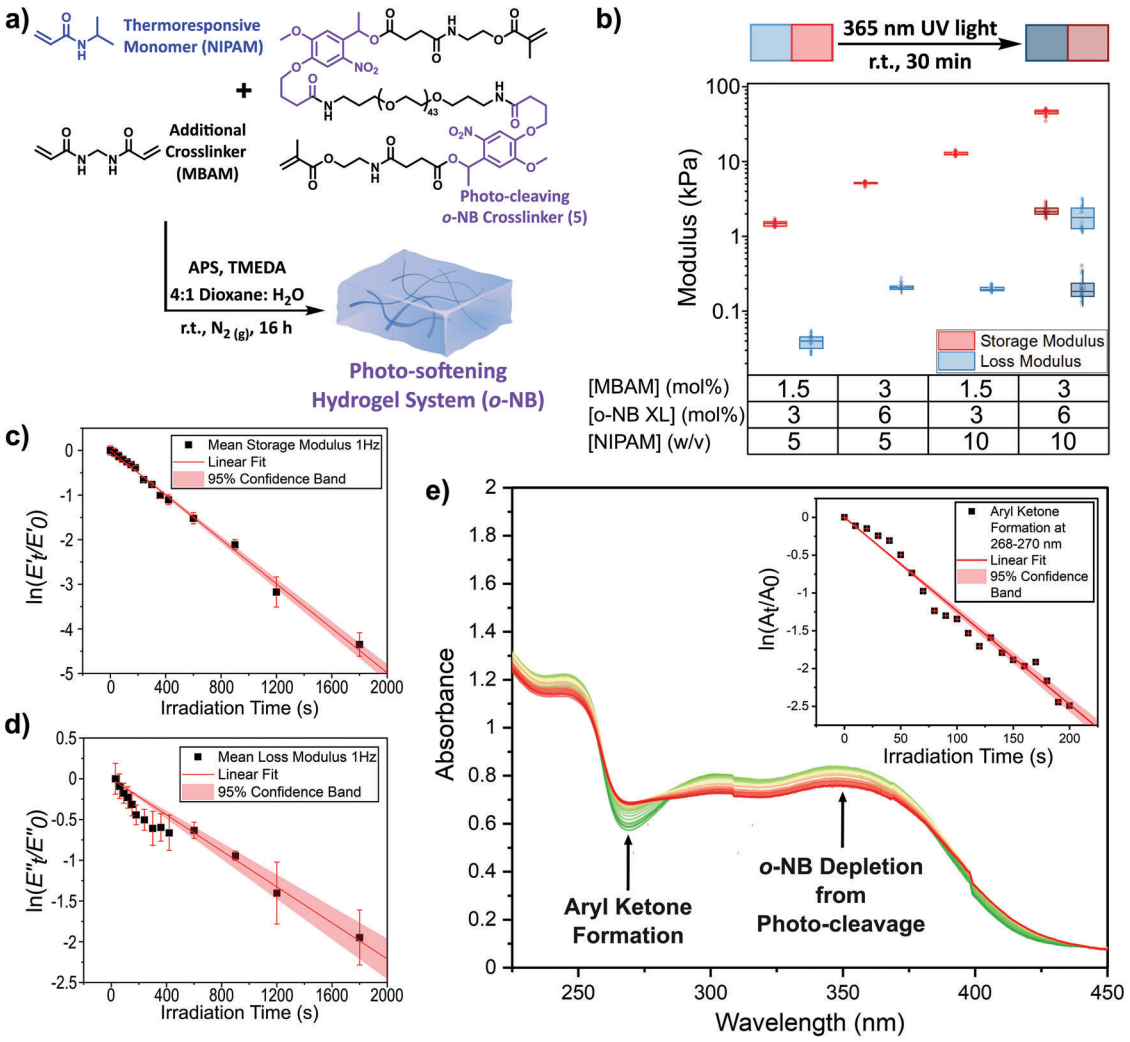

Figure 3. a) Scheme describing the synthesis of a photo-softening hydrogel (*o*-NB photo-cleavage) via the free radical polymerization of NIPAM, MBAM, and *o*-NB crosslinker (5) in the presence of APS and TMEDA. b) Box plot of storage (red) and loss (blue) moduli of 4 photo-softening hydrogels of differing compositions obtained from microindentation analysis. The lighter colored boxes represent pre-irradiation moduli, whereas the darker colored boxes show the storage and loss moduli after 30 min of irradiation at 365 nm (≈130 μW mm^{-2}). c,d) Microindentation kinetics study carried out on a 5 × 5 × 1 mm^3 photo-softening hydrogel, which was progressively irradiated with 365 nm UV light (≈130 μW mm^{-2}). In c), the natural logarithm of the change in storage modulus was plotted against irradiation time and fitted linearly with a R-squared value of 0.995. In d), the natural logarithm of the change in loss modulus plotted against time and fitted linearly with a R-squared value of 0.963. In both c) and d), the error bars represent the standard deviation between 4 measurements at each time point and the red bands are 95% confidence bands of the fittings. e) UV–vis kinetics study showing the changes in absorbance between 225–450 for a thin photo-softening hydrogel as a result of irradiation with 365 nm UV light (≈130 μW mm^{-2}) with 10 s increments for a total of 440 s. The color of the different spectra (green to red) highlights the time passed. *Inset*: The natural logarithm of the change in the average absorbance between 268–270 nm, corresponding to the formation of aryl ketone moieties (black squares), plotted against irradiation time (s). The experimental data points were fitted linearly (red line) with a R-squared value of 0.993. The red error bars represent the standard deviation between the absorbances at the 3 wavelengths at each time point, and the red band is a 95% confidence band of the fitting.

Similarly to the photo-stiffening hydrogel, we then used microindentation to carry out a kinetic study to determine the reaction kinetics of the photo-softening process within the hydrogel system. For this, a photo-softening hydrogel of dimensions 5 × 5 × 1 mm^3 was fabricated and anchored to a silane methacrylate-functionalized slide. Microindentation array measurements (2 by 2 array, 250 μm^2 area) were taken on the submerged, photo-softening hydrogel after different irradiation times with 365 nm light (irradiance of ≈130 μW mm^{-2}), for a total of 30 min. The natural logarithm of the ratio of storage or loss modulus over initial corresponding modulus [$ln(E'_t/E'_0)$ or $ln(E''_t/E''_0)$] when plotted against irradiation time gave linear plots (Figure 3c,d), thereby confirming that the hydrogel softening via *o*-NB crosslinker photo-cleavage was a 1st order process. This aligns well with previous kinetics studies conducted on the *o*-NB cleavage.[24,25] A control kinetics experiment was also performed with a non-photo-responsive hydrogel synthesized following the same method for the photo-softening hydrogel, but in place of the *o*-NB crosslinker (5), a non-photo-responsive PEG crosslinker (6) was used (Section S1.3.3.,

Supporting Information). The data depicted no significant softening of the hydrogel upon irradiation with 365 nm UV light (Figure S29c, Supporting Information), confirming that *o*-NB crosslinker (5) is critical for the photo-softening process of the hydrogel.

These data were then confirmed by a UV-Vis kinetic study on a new thin hydrogel (Figure S2, Supporting Information) fabricated directly on a silane-treated fused silica plate (Section S1.1.5., Supporting Information). UV–vis spectra were taken on the hydrogel immersed in MilliQ water, after different irradiation times with a 365 nm light (irradiance of ≈130 μW mm^{-2}), for a total of 440 s. (Figure 3e; Section S1.3.7., Supporting Information). At 0 s, the absorbance band of the *o*-NB moiety was observed (λ_{max} = 350 nm) (Figure 3e). As the irradiation time increased, the formation of the aryl ketone functionality (as a result of *o*-NB photo-cleavage) was observed at 270 nm. The absorbance band at 350 nm decreased over irradiation time, both as a result of the photochemical reaction and of the diffusion of the cleaved crosslinker out of the hydrogel film into the bulk solution. Importantly, the plot of $ln(A_{268\text{-}270\ nm,t}/A_{268\text{-}270\ nm,0})$ over irradiation time showed a linear correlation, confirming that the photo-cleavage process was 1st order. While the kinetic order of the photo-cleavage reaction was clearly confirmed as 1st order in both the microindentation and UV–vis kinetics experiments, the kinetic constants of the two studies are noticeably different. The UV–vis experiment showed that the reaction was completed in ≈200 s, whereas the indentation method showed that the reaction was completed in ≈20 min. As both kinetics studies were performed with identical irradiances, we ascribed the difference to the much smaller thickness of the hydrogel used in the UV–vis study. The thinner hydrogel was required in order to obtain accurate and resolved UV–vis spectra as thicker samples give absorbances above 1.5 that become broader due to light scattering.

2.3. Light-Induced Complex Actuation of a Hydrogel

As a first step toward the development of soft materials with mechanical properties that can be patterned and controlled with light, we used our photo-stiffening (*hν*DIBO) and photo-softening (*o*-NB) methodologies to develop a thermoresponsive hydrogel bilayer actuator, whose bending properties could be switched on with light (**Figure 4a**).

We started by characterizing the volume phase transition temperatures (VPTTs) of the photo-stiffening (*hν*DIBO) and photo-softening (*o*-NB) hydrogels. The VPTT of the two hydrogels were measured by monitoring the temperature-dependent volume changes of ≈3 × 3 × 1 mm^3 piece of pure photo-softening or photo-stiffening hydrogel (Section S1.4.1., Supporting Information). The VPPT of the photo-stiffening hydrogel was 28.8 ± 0.2 °C, while the VPTT of the photo-softening hydrogel was 35.4 ± 0.6 °C. Subsequently, we fabricated a soft bilayer actuator using a PMMA mold (20 × 5 × 1 mm^3) with one side (lengthwise) open to allow for the addition of the pre-gel solutions. In brief, first a photo-softening hydrogel layer was fabricated inside the mold. Subsequently, on top of the photo-softening hydrogel, a photo-stiffening hydrogel layer was placed, resulting in the hydrogel bilayer actuator shown in Figure 4b (Section S1.4.2., Supporting Information). Microindentation analysis was carried out on a ≈1.5 × 4 × 1 mm^3 cut piece of the bilayered soft actuator and used to produce storage and loss moduli heat maps of a cross-section of the material (Figure 4c, left). For this, 27 individual indentation measurements (3 by 9 array) were taken on an 800 μm by 3200 μm^2 area (400 μm spacings between measurements). Data analysis was carried out using our *ALIAS-Viscoelasticity* software, allowing us to obtain storage and loss moduli heat maps of the sample in ≈5 min. The photo-stiffening layer (bottom half) had average storage and loss moduli of 64.4 ± 4.8 kPa and 2.2 ± 0.4 kPa, respectively, whereas the photo-softening layer (top half) exhibited average storage and loss moduli of 129.9 ± 12.3 kPa and 3.9 ± 0.4 kPa, respectively. This showed that before irradiation the photo-softening hydrogel had ≈2 times higher elastic character than the photo-stiffening hydrogel. The effective diffusivity of the two hydrogel layers in the actuator were then determined, providing an indication of how quickly water diffuses through each polymer network (Section S1.4.3., Supporting Information). The photo-stiffening layer and the photo-softening layer had effective diffusivities of 2.66 ± 2.20 × 10^{-10} and 1.58 ± 2.77 × 10^{-10} m^2 s^{-1}, respectively. This data is consistent with the viscoelasticity properties of the two layers, indicating that in the photo-softening layer, the hydrogel swelling is restricted due to the higher *E'*, and, thus, the water diffusivity is reduced. Vice versa for the photo-stiffening layer.

Next, we studied the thermoresponsive actuation properties of the bilayer in water and observed that the material contracted reversibly and symmetrically upon temperature change between 20 and 60 °C (Figure 4b; Section S1.4.4., Supporting Information). Specifically, the hydrogel bilayer utilized for this experiment had initial dimensions of ≈18 × 4 × 1 mm^3 (average volume of 70.4 ± 0.3 mm^3) in MilliQ water and at 20 °C, whereas at 60 °C its dimensions decreased to ≈14 × 2.5 × 0.6 mm^3 (average volume of 19.7 ± 0.8 mm^3) with a 72 ± 1 vol% contraction. Importantly, the contraction was uniform and symmetric with a negligible change in the bilayer bending angle (Figure 4b). This contractile behavior was completely reversible, and the heating/cooling cycle could be repeated at least 20 times (Figure S33, Supporting Information). These thermoresponsive actuation properties were ascribed to the VPPTs of the two PNIPAM-based polymer networks.

We then employed UV light to turn on the temperature-dependent bending properties of the soft actuator. For this, the entire bilayer actuator was irradiated with a UV LED (356 nm, ≈130 μW mm^{-2}) for intervals of 5 and 20 min. This simultaneously caused the progressive photo-crosslinking of the photo-stiffening hydrogel layer, and the photo-decrosslinking of the photo-softening hydrogel layer. Microindentation mapping of the actuator cross-section interestingly showed that UV irradiation produced a progressive reversal of the viscoelastic properties of the two layers. Before irradiation, the photo-softening hydrogel layer (Figure 4c, top half) had higher storage and loss moduli than the photo-stiffening hydrogel layer (Figure 4c, bottom half), and upon UV irradiation, the viscoelastic properties of the two layers first became similar (after 5 min of irradiation), and finally, after 20 min of irradiation, they inverted. At the end of the experiment, the photo-stiffening hydrogel layer had higher storage and loss moduli (storage modulus = 121.0 ±

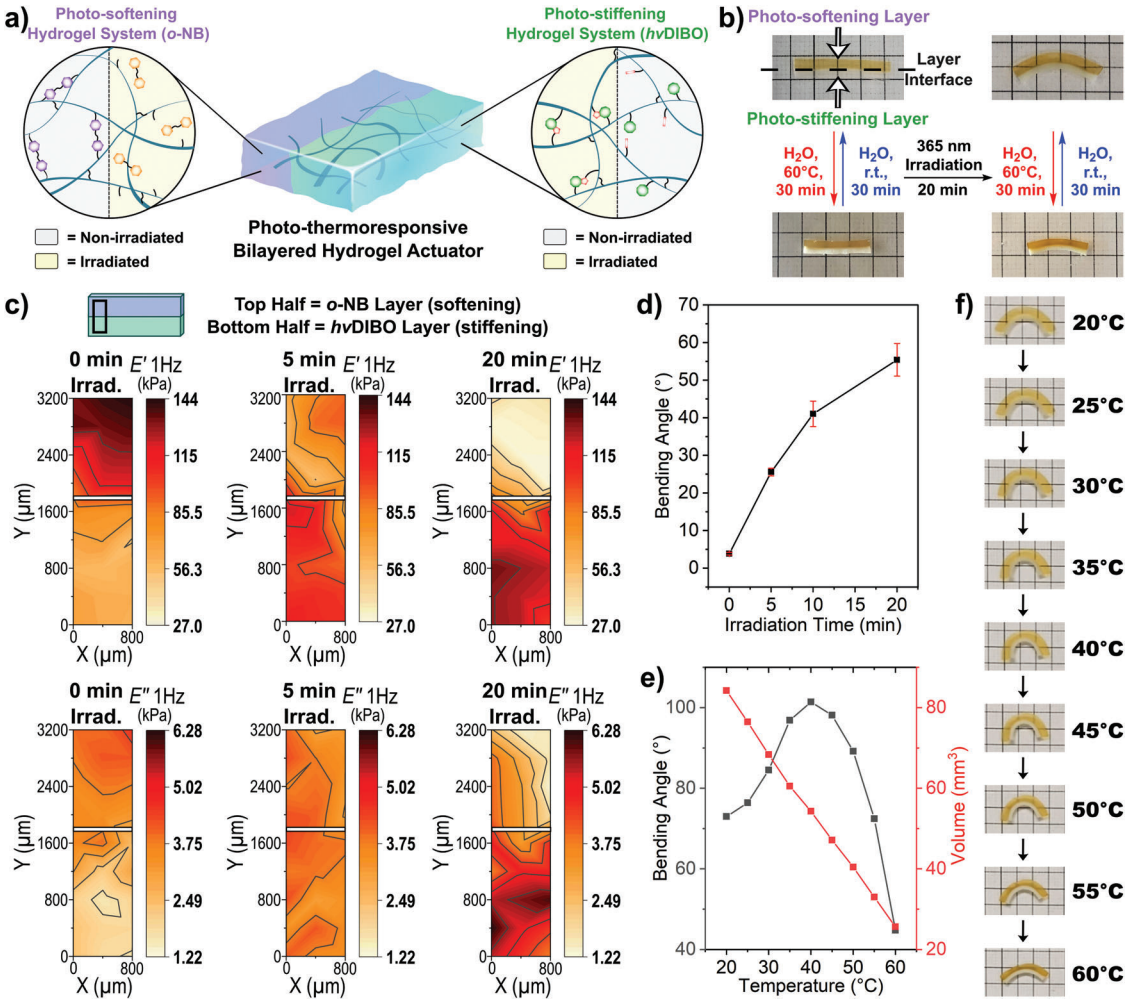

Figure 4. a) Scheme describing the structure, composition and photo-reactivity of the thermoresponsive bilayered hydrogel actuator. The blue lines inside the hydrogel representation depict the main PNIPAM polymer network and the small black lines in the magnified schemes are the MBAM crosslinks. The left layer (blue) represents the photo-softening hydrogel system capable of spatially and temporally softening via *ortho*-nitrobenzyl (*o*-NB) photo-cleavage reactions. The *o*-NB moieties (purple hexagons) can undergo intramolecular rearrangements with 365 nm light to form cleaved aryl ketones (orange hexagons). The right layer (green) represents the photo-stiffening hydrogel system capable of spatially and temporally stiffening via light-induced strain-promoted alkyne-azide cycloadditions (*hν*SPAAC) reactions. The *hν*DIBO groups (green octagons) can be unmasked with 365 nm light (≈130 μW mm^{-2}) and then they can crosslink with the azide groups (red rectangles). b) Photos of the bilayered actuator described in (a) and immersed in MilliQ water. The clear/white side is the photo-stiffening layer (*hν*DIBO) and the yellow/brown side is the photo-softening layer. The grid in the background is 5 × 5 mm^2. The two photos at the top show the bilayered actuator at 20 °C, before (left) and after (right) 20 min of irradiation with a 365 nm LED (≈130 μW mm^{-2}). The two photos at the bottom show instead the bilayered actuator at 60 °C, before (left) and after (right) UV irradiation. c) Top: Scheme of the bilayered actuator described in (a) and analyzed via microindentation. The small black rectangle superimposed to the hydrogel bilayer indicates the area of the material that was analyzed. Bottom: microindentation heat maps measuring the storage (top) and loss (bottom) moduli of a section of the bilayered actuator before irradiation (left), and after 5 min (middle) and 20 min of UV irradiation (right). The white lines at the center of the maps represent the boundary between the two hydrogel layers (top: photo-softening layer; bottom: photo-stiffening layer). Each map was the result of 27 indentation measurements (3 by 9 array) taken on an 800 by 3200 μm^2 area (400 μm spacings between measurements). d) Plot showing the actuator's bending angle (°) against UV irradiation time (min) for the hydrogel bilayer described in (a) and at 20 °C. The error bars represent the standard deviation between 3 measurements at each time point. e) Graph of the actuator's bending angle (°, black plot) and volume (mm^3, red plot) against temperature (°C, between 20 to 60 °C) for a 20 min UV irradiated actuator structure as described in (a). f) Time lapse images of the 20 min irradiated bilayered actuator described in (b) in MilliQ water when heated from 20 to 60 °C. The grid in the background is 5 × 5 mm^2.

9.8 kPa; loss modulus = 5.0 ± 0.8 kPa) than the photo-softening hydrogel layer (storage modulus = 37.6 ± 12.7 kPa; loss modulus = 2.4 ± 1.1 kPa). After 20 min of UV irradiation, the photo-stiffening layer also became less diffusible to water (effective diffusivity = 0.90 ± 0.39 × 10^{-10} m^2 s^{-1}) due to its denser polymer network, and the photo-softening layer became more diffusible to water (effective diffusivity = 2.22 ± 2.04 × 10^{-10} m^2 s^{-1}) due to a softer polymer network. Moreover, these measurements showed that within the experimental error of microindentation the mechanical properties of the sample were homogeneous throughout the thickness of each individual layer, with no evidence of a stiffness gradient due to light attenuation

through the depth of the sample during the irradiation process (Figure 4c).

During UV irradiation, we observed that the hydrogel bilayer started to bend toward the photo-stiffening layer (Figure 4d), indicating the triggering of the bending properties of the actuator. After 20 min of irradiation and at 20 °C, the hydrogel bilayer had a bending angle of 55° due to the swelling of the photo-softening hydrogel layer and the slight contraction of the photo-stiffening hydrogel layer (Figure 4b). Interestingly, while heating the 20 min irradiated bilayer to 60 °C, the actuator displayed a complex bending motion. First, the curvature of the bilayer rapidly increased to a bending angle of 101° at 40 °C, due to the fast contraction of the photo-stiffening layer. Then, the actuator started to straighten until it reached a bending angle of 45° at 60 °C (Figure 4e,f; Video S1, Supporting Information). Since we verified that 20 min of UV light irradiation *(i)* did not modify the VPTTs of the two hydrogel layers which, within experimental error, remained the same (VPTT for the photo-stiffening hydrogel = 28.5 ± 0.2 °C; VPTT for the photo-softening hydrogel = 36.1 ± 0.3 °C), and *(ii)* did not alter the overall volume contraction of the material, which remained able to contract by 72 ± 1%, we ascribed the complex bending motion of the material to the change in the viscoelastic properties of the two layers upon UV irradiation, and in particular to a marked difference in the speed of diffusion of water out of the two hydrogel layers.

Taken together, these results showed that our photo-stiffening and photo-softening hydrogels can be used to drastically modify a pattern of mechanical properties present on a soft material and trigger complex actuation mechanisms. This was demonstrated with the key support of microindentation analysis, which enabled the punctual and spatial characterization of the actuator's patterned viscoelastic and solvent diffusivity properties as a function of the irradiation time. From a general perspective, we showed the possibility of using light to break the fine balance between the mechanical properties of the two distinct layers of a hydrogel bilayer. This induced mechanical movement of the overall material as a consequence of the transduction of a light stimulus into the localized and simultaneous formation and cleavage of chemical bonds. The principles shown in this part of the work will open important applications not only in soft robotics, but also for the development of advanced substrates for tissue engineering.

2.4. Photo-Patterning of Digital Information Using Mechanical Properties

After demonstrating the utility of our photo-crosslinking and photo-decrosslinking hydrogels in switching on the bending capabilities of a soft actuator, we then explored the possibility of utilizing the same chemistry to encode mechanical property information in soft materials. As a first experiment, we fabricated a 5 × 5 × 1 mm^3 photo-stiffening hydrogel and applied on its top, a black photo-mask with the transparent text "*hv-DIBO*" (Section S1.5.1., Supporting Information). The masked hydrogel was irradiated with 365 nm light for 5 min (≈130 μW mm^{-2}) to spatially trigger the *hv*SPAAC reaction. After 5 min of UV irradiation the hydrogel became slightly yellow in color, in line with our previous observations. Importantly, after irradiation, the hydrogel still looked homogeneous, and no pattern was visible on the surface of the material. Subsequently, the microindenter was used to measure the viscoelastic properties across the entire hydrogel by performing a 4000 by 3000 μm^2 array of indentation measurements with lateral spacings of 66.7 μm (2806 individual indentation measurements in total). Also, data analysis was carried out using our *ALIAS-Viscoelasticity* software, allowing us to obtain in ≈4 h, storage and loss moduli heat maps of the entire hydrogel sample. **Figure 5a** shows the result of this experiment, and clearly demonstrates the effectiveness of the microindentation technique in revealing patterns of mechanical properties within a soft material. Specifically, the non-irradiated portion of the hydrogel had average E' and E'' values of 59.8 ± 7.4 and 2.71 ± 0.45 kPa, respectively, while the irradiated area ("*hv*-DIBO" pattern) had average E' and E'' values of 99.4 ± 10.3 and 5.74 ± 0.91 kPa, due to the extra crosslinking triggered using the photo-induced SPAAC reaction. The relative height profile of the material was calculated through the analysis of the same dataset, and it showed that the surface of the irradiated areas depressed by an average of 5.7 ± 0.6 μm compared to the non-irradiated hydrogel surface. We attributed this slight contraction of the irradiated portions of the material to the additional crosslinking of the hydrogel matrix, resulting in denser regions that are not able to swell as much as the surrounding areas.

We then tested the same principle using the photo-softening hydrogel system. For this, we fabricated a 10 × 10 × 1 mm^3 photo-softening hydrogel and applied on its top, a photo-mask with the transparent text "*o*-NB" (Section S1.5.2., Supporting Information). The system was then irradiated with 365 nm light for 20 min (≈130 μW mm^{-2}), to selectively trigger the photo-cleavage of the *o*-NB crosslinker (5) in the non-masked areas of the hydrogel. After 20 min of UV irradiation, the transparent, yellow hydrogel became a darker yellow color, in line with what was observed in our previous experiments. When the irradiated hydrogel was immersed in MilliQ water, the irradiated portion of the material slightly swelled and it was possible to recognize the "*o*-NB" text when the material was observed under a lamp and at an angle (Figure S35d, Supporting Information). An array of indentation measurements was then performed on an area of 7500 by 3000 μm^2 with lateral spacings of 100 μm.

The resulting 2356 individual indentation measurements were automatically analyzed using our *ALIAS-Viscoelasticity* analysis software to obtain storage and loss moduli heat maps in ≈3 h (Figure 5b). Similarly to the previous system, the microindentation array experiment allowed us to reveal the pattern of mechanical properties that were photo-patterned within the material. In particular, the non-irradiated area of the hydrogel had average E' and E'' values of 100.0 ± 8.2 and 8.65 ± 1.40 kPa, respectively, while the irradiated portions ("*o*-NB") had average E' and E'' values of 18.7 ± 6.5 and 1.90 ± 1.04 kPa. The relative height profile of the photo-patterned hydrogel revealed an average height increase of 29.7 ± 5.9 μm for the text compared to the parts of the material that were not irradiated. It seems that the reduction in crosslinking density, as a result of photo-cleavage of *o*-NB crosslinker (5), increased the ability of the hydrogel to swell, increasing its volume. On the basis of these encouraging results, we then utilized the same photo-patterning principles to encode digital information within a hydrogel in the form of spatially patterned, mechanical properties that are invisible to the

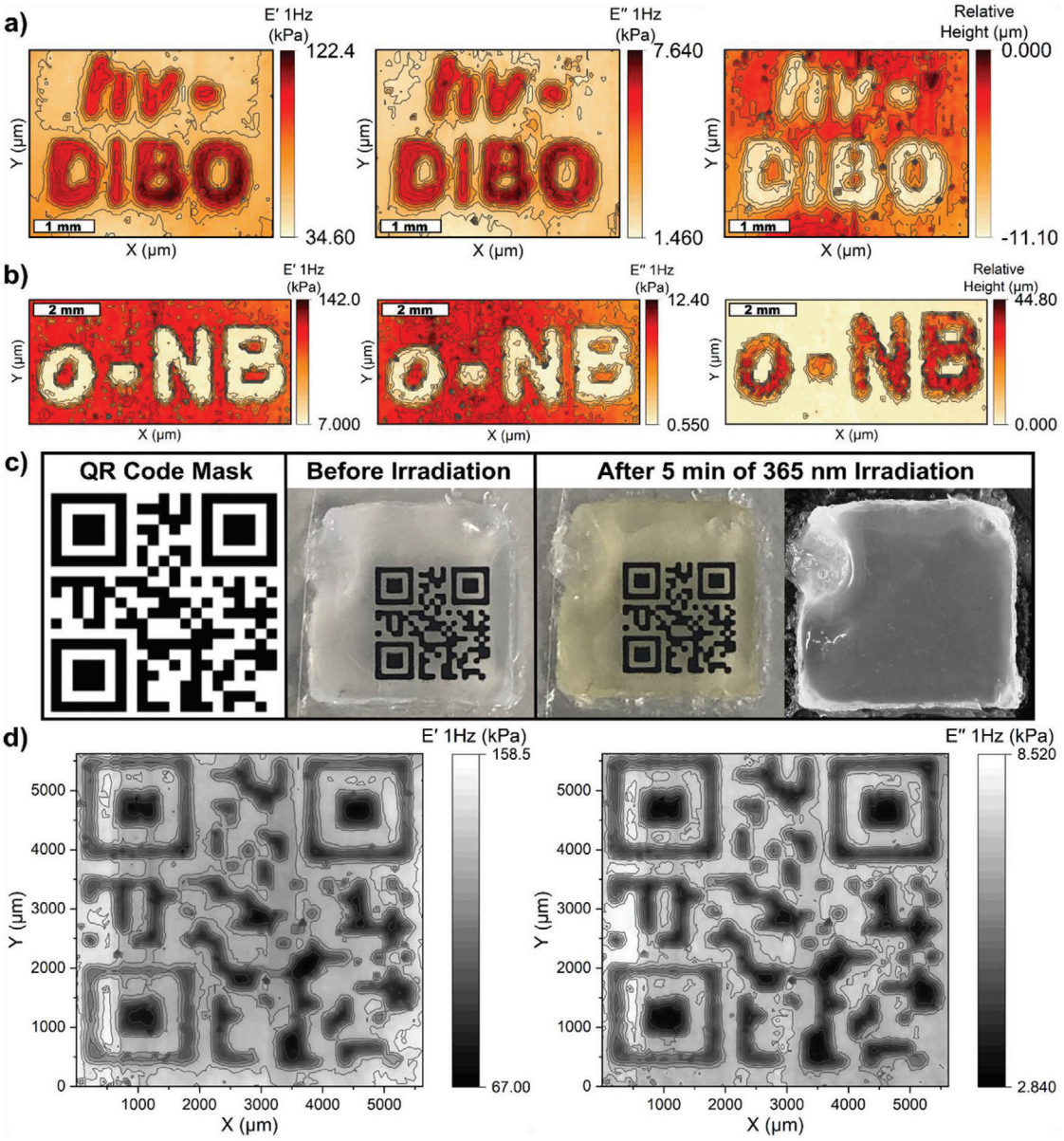

Figure 5. a) Microindentation storage (left) and loss (middle) moduli heat maps and relative height profile map (right) of a photo-patterned, photo-stiffening hydrogel ($5 \times 5 \times 1$ mm^3) (scale bar = 1 mm). The maps were obtained via the automated analysis of 2806 individual indentation curves (61 by 46 array) using our data analysis software *ALIAS-Viscoelasticity*. b) Microindentation storage (left) and loss (middle) moduli heat maps and relative height profile map (right) of a photo-patterned, photo-softening hydrogel ($10 \times 10 \times 1$ mm^3) (scale bar = 2 mm). The maps were obtained via the automated analysis of 2356 individual indentation curves (76 by 31 array) using our data analysis software *ALIAS-Viscoelasticity*. c) Left: QR code leading to www.gobbo-group.com that was used to make a photo-mask for a photo-stiffening hydrogel. Center left: Image of a photo-stiffening hydrogel ($10 \times 10 \times 1$ mm^3) with a QR-code photo-mask ($\approx 5.5 \times 5.5 \times 1$ mm^3) placed on top of it before UV irradiation. Center right: Image of the photo-stiffening hydrogel after 5 min of 365 nm UV irradiation. Right: image of the photo-patterned, photo-stiffening hydrogel after UV irradiation and without the photo-mask showing a homogenous hydrogel with an invisible photo-pattern. d) Microindentation storage (left) and loss (right) moduli heat maps of the photo-patterned hydrogel described in (c). The maps were obtained via the automated analysis of 5776 individual indentation curves (76 by 76 array, 75 μm spacing, 5625 by 5625 μm^2 area) using our data analysis software *ALIAS-Viscoelasticity*.

naked eye, yet detectable utilizing automated microindentation analysis. For this, we selected the photo-stiffening hydrogel system since it allowed for the photo-patterning of mechanical properties with minimal swelling differences between irradiated and non-irradiated areas (just 5.7 ± 0.6 μm), and consequently for the production of a completely invisible pattern.

A photo-stiffening hydrogel of $5.5 \times 5.5 \times 1$ mm^3 was fabricated and a mask featuring a QR code that leads to www.gobbo-group.com was placed on top of it (Figure 5c, left) (Section S1.5.3., Supporting Information). The hydrogel was then irradiated with 365 nm light for 5 min (≈ 130 μW mm^{-2}). Upon UV irradiation, the soft material became slightly yellow in color, but the patterned

QR code was invisible by the naked eye (Figure 5c, right). Microindentation was then used to map a 5625 by 5625 μm^2 area by performing a 76 by 76 array of dynamic force-relaxation measurements with 75 μm spacings. This yielded a dataset of 5776 individual force-relaxation curves in ≈8 h, which were automatically analyzed with our *ALIAS-Viscoelasticity* software to obtain storage and loss modulus heat maps. Figure 5d shows the results of the experiment and a well resolved QR code both for the storage and loss moduli maps that are detectable with a common smartphone. In particular, the non-irradiated portions of the hydrogel (QR code) had average E' and E'' values of 96.4 ± 11.6 and 4.38 ± 0.66 kPa, respectively, while the irradiated areas had average E' and E'' values of 132.2 ± 8.2 and 7.10 ± 0.36 kPa. The digital information in the form of patterned mechanical properties were therefore successfully encoded within the hydrogel.

From a general perspective, these results demonstrate that our photo-reactive hydrogels can be utilized to pattern mechanical properties within soft materials and to encode digital information that is invisible to the naked eye, but detectable using a microindenter as a micron-scale, highly sensitive, tactile sensor.

3. Conclusions

In this work we have developed two new types of photo-responsive and thermoresponsive PNIPAM-based hydrogels that allow for the patterning of mechanical properties for diverse applications. In the first hydrogel, we exploited the *hν*DIBO monomer (2) and a light-induced SPAAC reaction to crosslink the material and reinforce it. In the second hydrogel we exploited the PEG-based, *o*-NB crosslinker (5) and a photo-induced decrosslinking reaction to soften the soft material. The viscoelastic properties of the photo-stiffening and photo-softening hydrogels were characterized and optimized using microindentation. We also highlighted how microindentation can be used to follow the reaction kinetics of both hydrogel photo-crosslinking and photo-decrosslinking. From these experiments, it was possible to obtain key physical-organic chemistry information on the soft systems analyzed, such as the kinetic orders of the reactions and the apparent kinetic rate constants. Overall, this information was in good agreement with the kinetic constants for the same reactions obtained using a classical UV–vis spectroscopy method, even though the rate constants obtained using microindentation were always smaller than those obtained using UV–vis spectroscopy. We ascribed this to additional diffusion and polymer network rearrangement kinetic factors that can be detected via microindentation, but not through UV–vis spectroscopy.

By combining these two new hydrogel systems, we then showcased a potential application in the development of a soft actuator whose bending properties could be switched on with UV light. Initially, this bilayered system was only able to homogeneously and symmetrically contract due to the thermoresponsive properties of PNIPAM. However, after irradiation, the system started to bend at room temperature. By raising the temperature, the bending angle of the actuator increased until reaching 100° at 40 °C. After this temperature the actuator started to straighten until reaching a bending angle of 45° at 60 °C. Although in this experiment the entire actuator was irradiated, the observed complex bending behavior was ascribed to the difference in the effective diffusivities of the solvent through the two different types of polymer networks. In other words, a homogenous light irradiation of the entire material caused an asymmetrical change in the mechanical and diffusivity properties of the soft material, which triggered a different and more complex actuation mode. Symmetry could also be broken by harnessing the spatio-temporal control of light to locally switch on specific mechanical properties on a soft material and enable the fabrication of advanced soft actuators capable of even more complex forms of actuation. In the second part of the work, microindentation was key in characterizing the functioning mechanism of the actuator, as UV irradiation was found to not cause any change on the VPTT nor in the overall contraction of the material.

Finally, we showed that both hydrogel systems, and especially the photo-stiffening hydrogel, could be effectively utilized to store digital information in the form of patterned mechanical properties. The digital information, a QR code leading to a website, was invisible to the naked eye and could only be retrieved by mapping the entire material surface using the microindenter. Seeing the high number of individual indentation curves (> 5700) carried out to map the entire soft material surface, the automated data analysis performed by our software, *ALIAS-Viscoelasticity*, was key to retrieve the spatio-temporally encoded digital information.

From a general perspective, the methodologies developed and described in this work open up a route toward the development of new soft materials, displaying spatio-temporal patterns of mechanical properties. Such materials will find applications, not only for the development of advanced actuators and in digital information storage, but also in tissue engineering and biotechnology. For example, they could be used as advanced scaffolds for guiding the growth and differentiation of cells – since cells are very sensitive not only to chemical signals but also to mechanical stimuli;[26] or for studying the origin of specific diseases, such as cancer and fibrosis because they are associated with alterations in environmental stiffness.[27]

Supporting Information

Supporting Information is available from the Wiley Online Library or from the author.

Acknowledgements

The authors acknowledge funding from the Ontario Graduate Scholarship, NSERC (RGPIN-03859), the University of Bristol EPSRC Industrial and International Leverage Fund (EP/T517872/1), the EPSRC New Investigator Award (EP/T01508X/1), the European Union ERC (PROTOMAT, 101039578), and the project PRIN PNRR 3D-L-INKED (P2022BLNCS – financed by European Union Next Generation EU). Views and opinions expressed are those of the author(s) only and do not necessarily reflect those of the European Union or the European Research Council. Neither the European Union nor the granting authority can be held responsible for them. The authors also gratefully acknowledge the Electron and Scanning Probe Microscopy Unit of the University of Bristol for their support and assistance in this work. JHP thanks The University of Bristol and The University of Western Ontario for the opportunity provided by the cotutelle PhD program.

Open access publishing facilitated by Universita degli Studi di Trieste, as part of the Wiley - CRUI-CARE agreement.

Code Availability

The code that was developed to undertake the analysis presented in this work is provided in GitHub ("https://github.com/PierangeloGobbo1986/ALIAS-Viscoelasticity"), along with documentation on installation and use, and an example dataset.

Conflict of Interest

The authors declare no conflict of interest.

Data Availability Statement

The data that support the findings of this study are available from the corresponding author upon reasonable request.

Keywords

Hydrogel, indentation, mechanical properties, photo-click chemistry, spatio-temporal pattern

Received: September 20, 2024
Revised: October 8, 2024
Published online:

[1] a) C. Huang, D. Quinn, S. Suresh, K. J. Hsia, *P. Natl. Acad. Sci. U. S. A.* **2018**, *115*, 70; b) J. E. Meiring, S. Lee, E. A. Costner, M. J. Schmid, T. B. Michaelson, C. G. Willson, S. M. Grayson, *Opt. Eng.* **2009**, *48*, 037201; c) F. Amir, K. P. Liles, A. O. Delawder, N. D. Colley, M. S. Palmquist, H. R. Linder, S. A. Sell, J. C. Barnes, *ACS Appl. Mater. & Interfaces* **2019**, *11*, 24627; d) A. Singh, A. N. Shi, S. A. Claridge, *Chem. Commun.* **2022**, *58*, 13059.

[2] a) E. R. Ruskowitz, C. A. DeForest, *Nat. Rev. Mater.* **2018**, *3*, 17087; b) M. Lee, R. Rizzo, F. Surman, M. Zenobi-Wong, *Chem. Rev.* **2020**, *120*, 10950; c) J. J. Boland, *Nat. Mater.* **2010**, *9*, 790; d) P. Rothemund, Y. Kim, R. H. Heisser, X. H. Zhao, R. F. Shepherd, C. Keplinger, *Nat. Mater.* **2021**, *20*, 1582; e) H. Peng, Y. M. Xin, J. Xu, H. Z. Liu, J. Y. Zhang, *Mater. Horiz.* **2019**, *6*, 618; f) V. Magdanz, S. Sanchez, O. G. Schmidt, *Adv. Mater.* **2013**, *25*, 6581; g) X. Liu, K. Zhao, T. Gong, J. Song, C. Bao, E. Luo, J. Weng, S. Zhou, *Biomacromolecules* **2014**, *15*, 1019; h) A. Kirillova, R. Maxson, G. Stoychev, C. T. Gomillion, L. Ionov, *Adv. Mater.* **2017**, *29*, 1703443; i) O. O. Akintewe, S. J. DuPont, K. K. Elineni, M. C. Cross, R. G. Toomey, N. D. Gallant, *Acta Biomater.* **2015**, *11*, 96; j) E. Gultepe, J. S. Randhawa, S. Kadam, S. Yamanaka, F. M. Selaru, E. J. Shin, A. N. Kalloo, D. H. Gracias, *Adv. Mater.* **2013**, *25*, 514; k) F. Gabler, D. D. Karnaushenko, D. Karnaushenko, O. G. Schmidt, *Nat. Commun.* **2019**, *10*, 3013.

[3] a) G. A. Primo, A. Mata, *Adv. Funct. Mater.* **2021**, *31*, 2009574; b) E. R. Hui, J. L. Sumey, S. R. Caliari, *Mol. Syst. Des. Eng.* **2021**, *6*, 670; c) T. E. Brown, K. S. Anseth, *Chem. Soc. Rev.* **2017**, *46*, 6532.

[4] a) C. Ligorio, A. Mata, *Nat. Rev. Bioeng.* **2023**, *1*, 518; b) A. Aazmi, D. Zhang, C. Mazzaglia, M. Yu, Z. Wang, H. Yang, Y. Y. S. Huang, L. Ma, *Bioact. Mater.* **2024**, *31*, 475; c) A. S. Pellowe, A. L. Gonzalez, *Wires Nanomed. Nanobi.* **2016**, *8*, 5; d) X. Y. Ma, X. Qu, W. Zhu, Y. S. Li, S. L. Yuan, H. Zhang, J. Liu, P. R. Wang, C. S. E. Lai, F. Zanella, G. S. Feng, F. Sheikh, S. Chien, S. C. Chen, *Proc. Natl. Acad. Sci. U.S.A.* **2016**, *113*, 2206; e) D. Joung, V. Truong, C. C. Neitzke, S.-Z. Guo, P. J. Walsh, J. R. Monat, F. Meng, S. H. Park, J. R. Dutton, A. M. Parr, M. C. McAlpine, *Adv. Funct. Mater.* **2018**, *28*, 1801850; f) I. M. Tayler, R. S. Stowers, *Acta Biomater.* **2021**, *132*, 4; g) O. Chaudhuri, J. Cooper-White, P. A. Janmey, D. J. Mooney, V. B. Shenoy, *Nature* **2020**, *584*, 535; h) A. Bhusal, E. Dogan, D. Nieto, S. A. Mousavi Shaegh, B. Cecen, A. K. Miri, *ACS Appl. Bio Mater.* **2022**, *5*, 4480; i) R. Mateen, M. M. Ali, T. Hoare, *Nat. Commun.* **2018**, *9*, 602; j) R. S. Stowers, S. C. Allen, L. J. Suggs, *Proc. Natl. Acad. Sci. U.S.A.* **2015**, *112*, 1953; k) A. Jagiełło, Q. Hu, U. Castillo, E. Botvinick, *Acta Biomater.* **2022**, *141*, 39.

[5] a) C. Gong, Y. Zhai, J. Zhou, Y. Wang, C. Chang, *J. Mater. Chem. C.* **2022**, *10*, 549; b) Y. Ma, S. Ma, W. Yang, B. Yu, X. Pei, F. Zhou, W. Liu, *Adv. Mater. Technol.* **2019**, *4*, 1800467; c) H. Yuk, S. Lin, C. Ma, M. Takaffoli, N. X. Fang, X. Zhao, *Nat. Commun.* **2017**, *8*, 14230; d) J. Li, L. Dekanovsky, B. Khezri, B. Wu, H. Zhou, Z. Sofer, *Cyborg Bionic Syst* **2022**, *2022*, 824057.

[6] a) Y. Sun, X. X. Le, S. Y. Zhou, T. Chen, *Adv. Mater.* **2022**, *34*, 2201262; b) P. Mohankumar, J. Ajayan, T. Mohanraj, R. Yasodharan, *Measurement* **2021**, *167*, 108293.

[7] a) M. Guvendiren, M. Perepelyuk, R. G. Wells, J. A. Burdick, *J. Mech. Behav. Biomed.* **2014**, *38*, 198; b) A. M. Kloxin, M. W. Tibbitt, A. M. Kasko, J. A. Fairbairn, K. S. Anseth, *Adv. Mater.* **2010**, *22*, 61; c) A. M. Kloxin, A. M. Kasko, C. N. Salinas, K. S. Anseth, *Science* **2009**, *324*, 59; d) A. M. Rosales, S. L. Vega, F. W. DelRio, J. A. Burdick, K. S. Anseth, *Angew. Chem., Int. Ed.* **2017**, *56*, 12132; e) S. C. P. Norris, P. Tseng, A. M. Kasko, *ACS Biomater. Sci. Eng.* **2016**, *2*, 1309.

[8] a) R. Prevedel, A. Diz-Muñoz, G. Ruocco, G. Antonacci, *Nat. Methods* **2019**, *16*, 969; b) C. Bevilacqua, J. M. Gomez, U.-M. Fiuza, C. J. Chan, L. Wang, S. Hambura, M. Eguren, J. Ellenberg, A. Diz-Muñoz, M. Leptin, R. Prevedel, *Nat. Methods* **2023**, *20*, 755; c) G. J. Pahapale, J. Tao, M. Nikolic, S. Gao, G. Scarcelli, S. X. Sun, L. H. Romer, D. H. Gracias, *Adv. Sci.* **2022**, *9*, 2104649; d) A. M. Eltony, P. Shao, S.-H. Yun, *Nat. Commun.* **2022**, *13*, 1354.

[9] A. E. Chalard, A. W. Dixon, A. J. Taberner, J. Malmström, *Front. Cell Dev. Biol.* **2022**, *10*, 946754.

[10] O. H. Olubowale, S. Biswas, G. Azom, B. L. Prather, S. D. Owoso, K. C. Rinee, K. Marroquin, K. A. Gates, M. B. Chambers, A. Xu, J. C. Garno, *ACS Omega* **2021**, *6*, 25860.

[11] A. A. Poloukhtine, N. E. Mbua, M. A. Wolfert, G.-J. Boons, V. V. Popik, *J. Am. Chem. Soc.* **2009**, *131*, 15769.

[12] a) M. Bjerknes, H. Cheng, C. D. McNitt, V. V. Popik, *Bioconjug. Chem.* **2017**, *28*, 1560; b) C. M. Madl, Y. X. Wang, C. A. Holbrook, S. Su, X. Shi, F. J. Byfield, G. Wicki, I. A. Flaig, H. M. Blau, *Proc. Natl. Acad. Sci. U.S.A.* **2024**, *121*, 2406787121.

[13] M. P. O'Hagan, Z. J. Duan, F. J. Huang, S. Laps, J. T. Dong, F. Xia, I. Willner, *Chem. Rev.* **2023**, *123*, 6839.

[14] K. Nakayama, T. Tachikawa, T. Majima, *Langmuir* **2008**, *24*, 6425.

[15] a) Y. N. Zhang, C. H. Fang, W. S. P. Carvalho, Y. F. Gao, M. J. Serpe, *ACS Appl. Polym. Mater.* **2021**, *3*, 410; b) J. Z. Liu, W. R. Kang, W. P. Wang, *Photochem. Photobiol.* **2022**, *98*, 288; c) D. R. Griffin, A. M. Kasko, *ACS Macro Lett.* **2012**, *1*, 1330.

[16] a) C. W. H. Rajawasam, C. Tran, M. Weeks, K. S. McCoy, R. Ross-Shannon, O. J. Dodo, J. L. Sparks, C. S. Hartley, D. Konkolewicz, *J. Am. Chem. Soc.* **2023**, *145*, 5553; b) C. A. Garrido, D. S. Garske, M. Thiele, S. Amini, S. Real, G. N. Duda, K. Schmidt-Bleek, A. Cipitria, *Biomater. Adv.* **2023**, *151*, 213423.

[17] a) Z. Chen, Y. J. Chen, Y. T. Guo, Z. Yang, H. Li, H. Z. Liu, *Adv. Funct. Mater.* **2022**, *32*, 2201009; b) Y. H. Ye, Z. Y. Yu, Y. F. Zhang, F. Jiang, *Mater. Horiz.* **2023**, *10*, 2667; c) A. Abdollahi, H. Roghani-Mamaqani, B. Razavi, M. Salami-Kalajahi, *ACS Nano* **2020**, *14*, 14417; d) X. F. Ji, R. T. Wu, L. L. Long, X. S. Ke, C. X. Guo, Y. J. Ghang, V. M. Lynch, F. H. Huang, J. L. Sessler, *Adv. Mater.* **2018**, *30*, 1705480; e) C. H. Zhu, L. Zhang, A. Zou, W. W. Wang, J. H. Zhang, A. M. Zhang, *Chem. Eng. J.* **2023**, *475*, 146161.

[18] W. Luo, J. Luo, V. V. Popik, M. S. Workentin, *Bioconjug. Chem.* **2019**, *30*, 1140.

[19] S. Arumugam, V. V. Popik, *J. Org. Chem.* **2014**, *79*, 2702.

[20] S. Nainar, M. Kubota, C. McNitt, C. Tran, V. V. Popik, R. C. Spitale, *J. Am. Chem. Soc.* **2017**, *139*, 8090.
[21] C. D. McNitt, H. Cheng, S. Ullrich, V. V. Popik, M. Bjerknes, *J. Am. Chem. Soc.* **2017**, *139*, 14029.
[22] P. J. Grimes, M. Jenkinson-Finch, H. E. Symons, W. H. Briscoe, S. Rochat, S. Mann, P. Gobbo, *Chem. - Eur. J.* **2023**, 202302058.
[23] a) L. Li, J. M. Scheiger, P. A. Levkin, *Adv. Mater.* **2019**, *31*, 1807333; b) Y. H. Xing, B. H. Zeng, W. Yang, *Front. Bioeng. Biotechnol.* **2022**, *10*, 1075670.
[24] P. Klan, T. Solomek, C. G. Bochet, A. Blanc, R. Givens, M. Rubina, V. Popik, A. Kostikov, J. Wirz, *Chem. Rev.* **2013**, *113*, 119.
[25] A. P. Pelliccioli, J. Wirz, *Photochem. Photobiol. Sci.* **2002**, *1*, 441.
[26] F. Serwane, A. Mongera, P. Rowghanian, D. A. Kealhofer, A. A. Lucio, Z. M. Hockenbery, O. Campàs, *Nat. Methods* **2017**, *14*, 181.
[27] a) N. F. Boyd, Q. Li, O. Melnichouk, E. Huszti, L. J. Martin, A. Gunasekara, G. Mawdsley, M. J. Yaffe, S. Minkin, *PLoS One* **2014**, *9*, 100937; b) J. Zhang, C. A. Reinhart-King, *Cancer Cell* **2020**, *37*, 754; c) R. G. Wells, *Biochim. Biophys. Acta Mol. Basis Dis.* **2013**, *1832*, 884.